Supporting Information

Study of strain engineered MoS_2 and its application in lactic acid biosensor

*Wenzhao Wang,*a Junyan Ou,a Xi Wang,a Zhongyue Luo,a Mingcong He,a Yinshan Zhu,a Da Wan,*a Qiongdi Zhang,a and Xiangbin Zeng,*b*

[a] School of Electronic Information, Wuhan University of Science and Technology, Wuhan 430081, China

[b] School of Integrated Circuits, Huazhong University of Science and Technology, Wuhan 430074, China

* wenzhaowang@wust.edu.cn, wanda@wust.edu.cn, eexbzeng@hust.edu.cn

The fabrication process of MS structure devices is shown in Figure S1. First, an electrode pattern is formed on the SiO_2/Si substrate by photolithography, including spin coating of AZ5214 photoresist, two ultraviolet exposures and development steps. Then, Ti/Au electrodes (10 nm/100 nm) are deposited by electron beam evaporation. Finally, the final electrode pattern is obtained by photoresist removal.

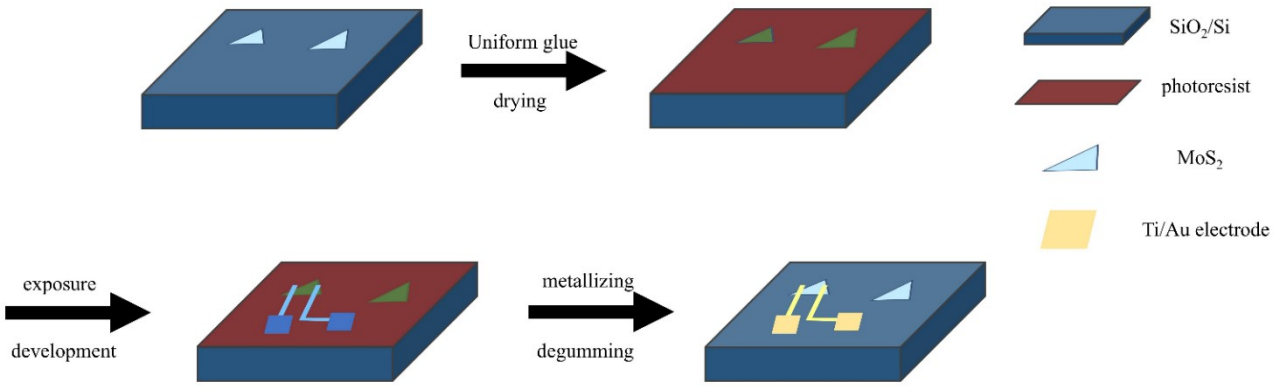

Figure S1. Flowchart of MS structural component fabrication process

The fabrication process of p-n junction devices is shown in Figure S2. It is achieved through three photolithography processes: first, gold markers are prepared as alignment references, then a doping mask is formed and oxygen plasma doping is performed, and finally electrode patterning and deposition are completed to obtain homojunction p-n devices.

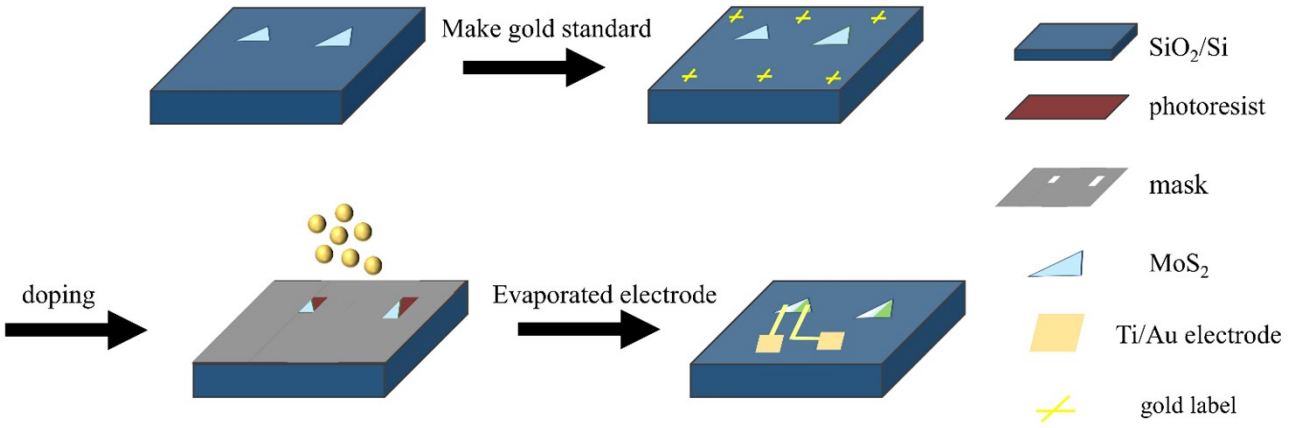

Figure S2. Flowchart for fabricating horizontal homogeneous p-n junctions

The wet transfer process of MoS_2 to the PET substrate is shown in Figure S3. PMMA is used as the support layer. The process involves spin coating and curing, etching and peeling with NaOH solution, cleaning with deionized water to remove residues, and removing PMMA with acetone and isopropanol. Finally, the complete transfer of MoS_2 to the PET substrate is achieved.

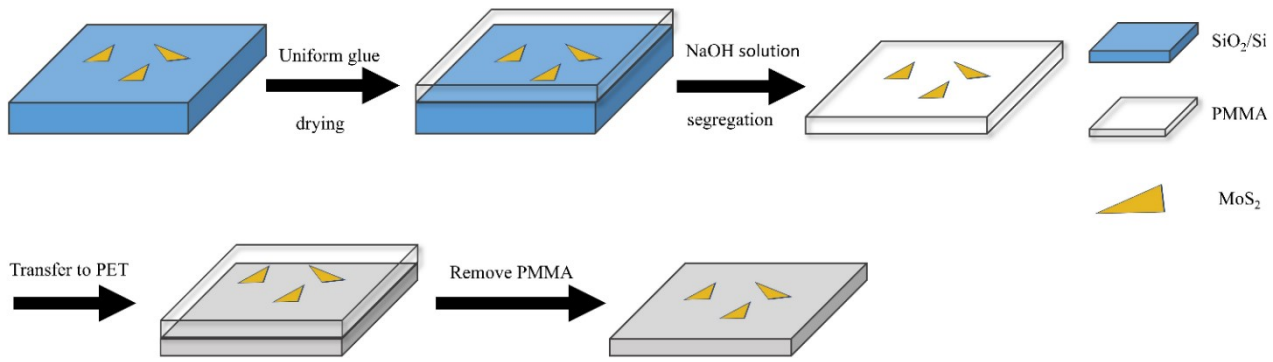

Figure S3. Wet transfer process flowchart

Figure S4 shows that the experimental data agree well with the linear model. This not only indicates that the thermionic emission-diffusion model is the main operating process of the device, but also shows that the theory can be used to extract the Schottky barrier from the experimental data.

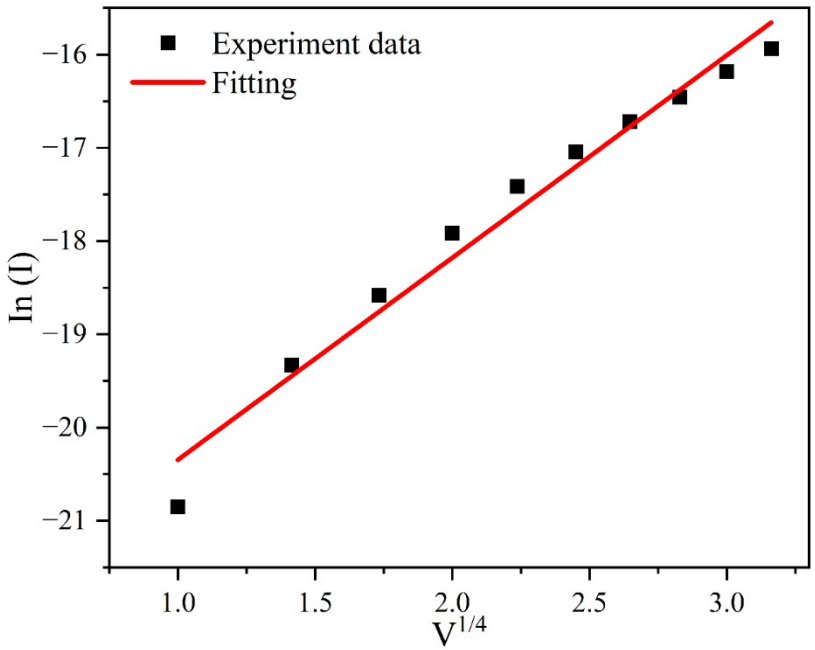

Figure S4. lnI-$V^{1/4}$ function fitted with unstrained I-V curve

Figure S5 shows the current response of the flexible MS structure sensor to glucose, uric acid, and lactic acid solutions (1 μM) in the unstretched state. The results indicate that the sensor's response to lactic acid is more significant. This is because the MoS_2 channels modified with lactate dehydrogenase and NAD^+ can specifically recognize lactate molecules and react with them to generate H^+, exhibiting good selectivity.

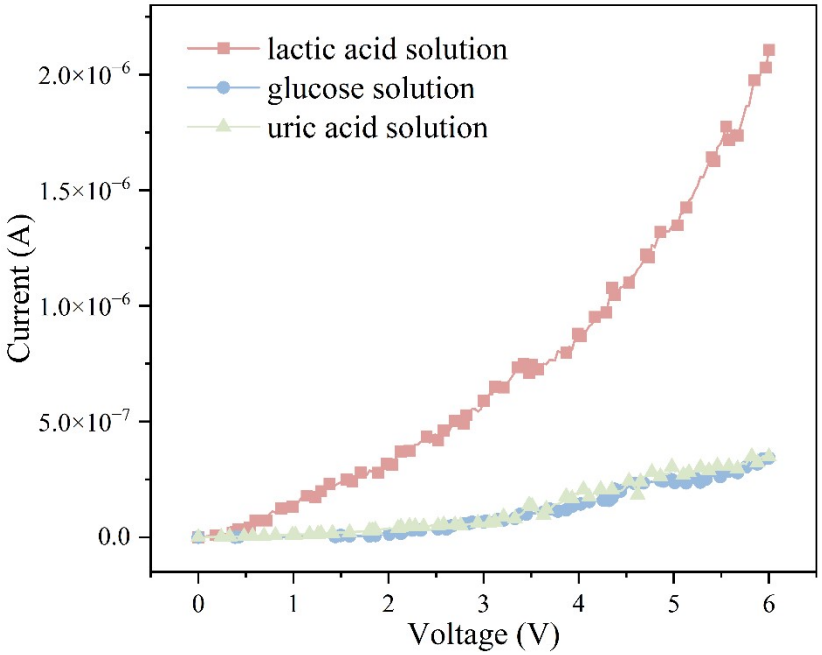

Figure S5. Selective response of the flexible device to glucose, uric acid, and lactic acid (1 μM) in its unstretched state.

Figure S6 shows the current response of the flexible MS structure sensor to artificial sweat（PH = 4.3) under different degrees of stretching. As can be seen from Figure S6, its response trend is basically consistent with the test results using PBS buffer in Figure 6(a) of the main text, which preliminarily verifies the applicability of the sensor in more complex media.

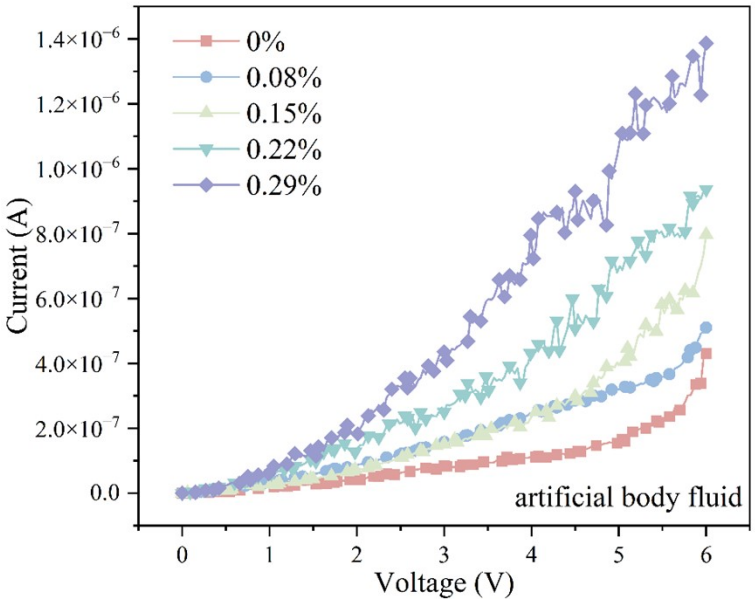

Figure S6. Current response of the flexible device to artificial sweat under various tensile strains.

We performed the I-V measurements to the flexible MS structured MoS_2 biosensor in PBS solution under duration of 0 to 15 days (Figure S7). At a voltage of 6V, after 15 days, the current ratio to the current after 0 days is 93.43%, indicating good stability of the device.

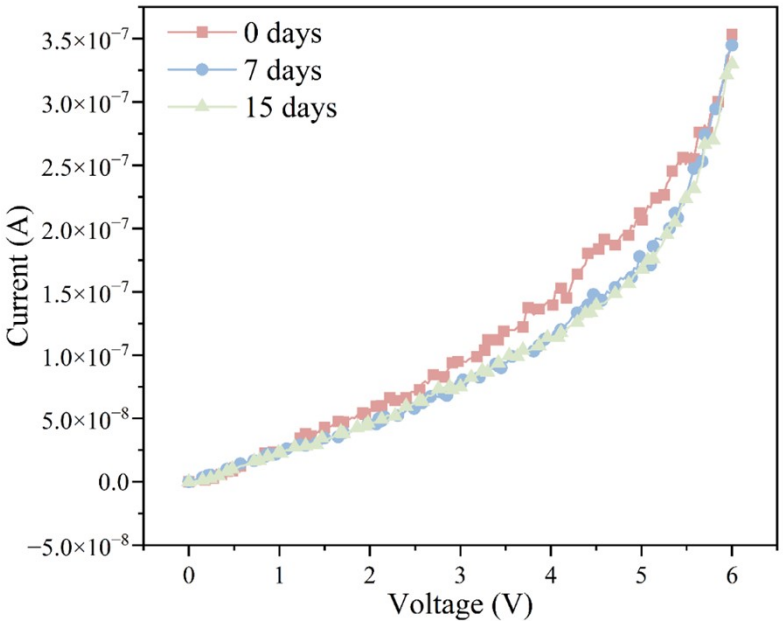

Figure S7. I-V response characteristics of flexible device to PBS solution at different days.

Figure S8 shows the electrical response characteristics of the flexible MS structure sensor in the unstretched state to 0–20 mM lactic acid solutions. The figure presents its I-V characteristic curves and the current change fitting curve calculated based on them. The results show that the sensor has a good linear response within this concentration range. Through linear fitting analysis, we obtained a high correlation coefficient (R^2 = 0.98602), which verifies the sensor's application potential for quantitative detection within physiologically relevant concentration ranges.

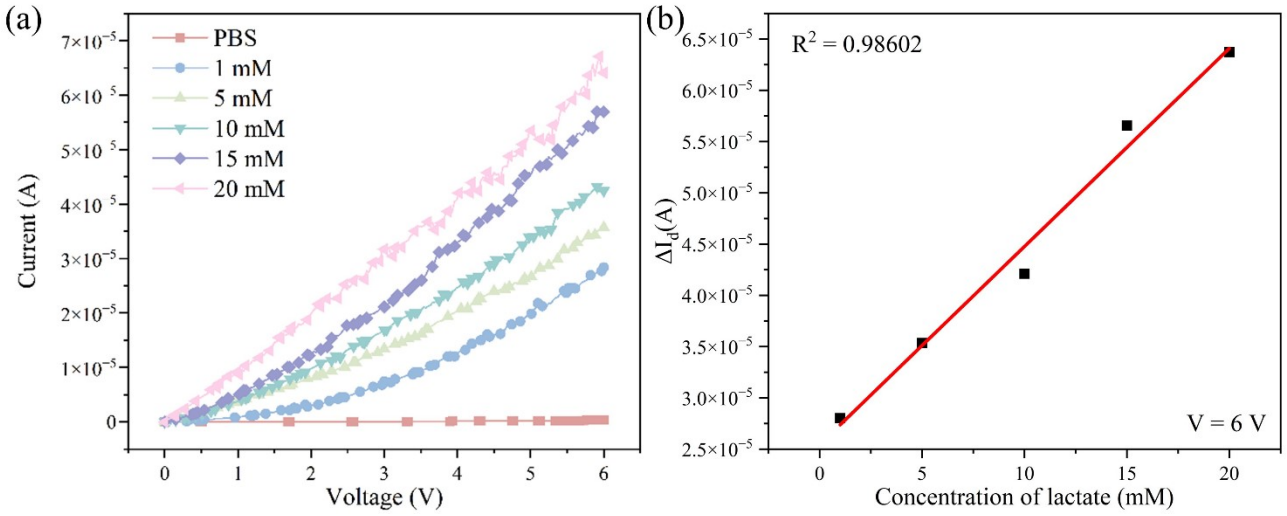

Figure S8. (a) I-V characteristic curves of flexible device for different concentrations of lactic acid in unstretched state. (b) Fitted curves of current change of the flexible device under different lactic acid concentrations.